Role of the Exciton-Polariton in a Continuous-Wave Optically Pumped CsPbBr₃ Perovskite Laser

Qiuyu Shang[1], Meili Li[1], Liyun Zhao[1], Dingwei Chen[2], Shuai Zhang[3], Shulin Chen[4], Peng Gao[4], Chao Shen[2], Jun Xing[5], Guichuan Xing[6], Bo Shen[7, 8], Xinfeng Liu[3], Qing Zhang[1, 8, *]

[1]Department of Materials Science and Engineering, College of Engineering, Peking University, Beijing 100871, China

[2]State Key Laboratory of Superlattices and Microstructures, Institute of Semiconductors, Chinese Academy of Sciences, Beijing 100083, China

[3]CAS Key Laboratory of Standardization and Measurement for Nanotechnology, CAS Center of Excellence for Nanoscience, National Center for Nanoscience and Technology, Beijing 100190, China

[4]Electron Microscopy Laboratory, International Center for Quantum Materials, School of Physics, Peking University, Beijing 100871, China

[5]Key Laboratory of Eco-Chemical Engineering, Ministry of Education, College of Chemistry and Molecular Engineering, Qingdao University of Science and Technology, Qingdao 266042, China

[6]Joint Key Laboratory of the Ministry of Education, Institute of Applied Physics and Materials Engineering, University of Macau, Avenida da Universidade Taipa 999078, Macao, SAR, China

[7]School of Physics, Peking University, Beijing 100871, China

[8]Research Center for Wide Gap Semiconductor, Peking University, Beijing 100871, China

Corresponding*: Q_zhang@pku.edu.cn

Table of Contents

Table S1. A comparison of our work with CW pumped laser based on perovskite materials in previous literatures.

Note S1. Fabrication and characterization

Samples fabrication and structural characterization. To synthesize CsPbBr$_3$ NBs on a glass substrate using the solution-processed method, CsBr and PbBr$_2$ powders (CsBr, 99.99%, Sigma Aldrich; PbBr$_2$, 99.99%, Sigma Aldrich) with a molar ratio of 1:1 are firstly mixed and then dissolved into 5 mL dimethyl formamide as precursors. The precursor solution is further dropped onto the glass substrate and placed into a Petri dish. The dish loaded glass substrate is ulteriorly nested into a beaker containing anti-solvents. The anti-solvent is a mixed solution of toluene and dichloromethane. In addition, the beaker needs to be sealed and tens of small holes (40–60) on the top needed to be made to control the evaporation of anti-solvents. Finally, the sealed beaker is placed into an oven, and the reaction temperature is set to 30–40 °C. After a growth time of 24 hours, the CsPbBr$_3$ NBs could be obtained. The CsPbBr$_3$ NBs could be further transferred onto sapphire, silver (5 nm silica on the surface), and silicon substrates via a dry method. A scanning electron microscope (SEM, Hitachi, S4800), X-ray diffraction (XRD, Rigaku, SmartLab 9KW), and a transmission electron microscope (TEM, FEI Tecnai F20) are utilized to characterize the morphology and crystalline structures of as-synthetized CsPbBr$_3$ NBs.

Optical spectroscopy. Temperature-dependent steady-state PL spectrum is obtained under a CW 405 nm solid-state laser in a cryostat (Cryo industry) under vacuum of 10^{-6} mbar by employing home-built fluorescence microscopy. The laser spot, with a diameter of ~28 μm, is focused onto individual NBs through a 50 × objective lens (NA = 0.5). The in-situ CW laser emission in Figure 1 and distal PL spectra in Figure 2 in the main text are measured using the same objective lens and further collected into a monochromator (Horiba, iHR550) equipped with a liquid nitrogen cooled charge coupled device (CCD) detector. The excitation laser line is blocked by a 405 nm long-pass filter. A 400 nm femtosecond pulsed laser is utilized to obtain temperature-dependent lasing spectra; the laser is frequency-doubled using a Coherent Libra regenerative amplifier of 800 nm (pulse duration: 80 fs, repetition rate: 1 kHz) via a BBO crystal. The excitation laser spot, with a diameter of ~30 μm, is focused onto individual NBs via a 50 × objective lens. For TRPL spectroscopy to probe the recombination channel and lifetime, a frequency-doubled 400 nm pulsed laser beam from Coherent Mira 900 (pulse duration: 120 fs,

800 nm, repetition rate: 76 MHz) is focused onto individual CsPbBr$_3$ NBs; the signal is analyzed using a time-correlated single-photon counting spectrometer (PicoQuant Hydraharp 400&id100-SMF20).

Note S2. Estimation of excitation density and current density

Excitation density. Optical pumped excitation density (N_e) under a power density of P can be calculated by:[1]

$$N_e = \frac{P\tau(1-R)(1-\exp(-\alpha d))}{\hbar\omega d} \qquad (1)$$

with τ the recombination lifetime (5 ns here), R the reflection coefficient, α the absorption coefficient ($\sim10^4$ cm^{-1}) at 405 nm, d the thickness settled as the dominant height of 120 nm here for simplicity, and $\hbar\omega$ the excitation energy (405 nm, 4.9×10^{-19} J). Eventually, N_e equals P based on 1.0 kW cm^{-2} = 0.8×10^{17} cm^{-3}.

Current density. The electrically injected current density (J) equals a excitation density of N_e can be calculated by:[2]

$$J = \frac{eN'd}{\tau} = \frac{eN_e\eta_{out}\eta_{PLQY}d}{\tau\eta_{EQE}} \qquad (2)$$

where e is the free electron charge, d is the thickness settled as the dominant height of 120 nm here for simplicity, N' is electrically injected carrier density, η_{EQE} is external quantum efficiency, $\eta_{out} = 1/(2\,n_r^2)$ is light out-coupling efficiency (n_r = 2.3, the bulk refractive index for CsPbBr$_3$), and η_{PLQY} is PL quantum yield. Herein, η_{EQE} is < 0.1% regarding the Auger recombination under current density > 100 A cm^{-2}.[2] Using parameters of η_{EQE} ~0.1%, η_{out} = 10%, and η_{PLQY} ~70%, an electrically injected current density of ~5.6 kA cm^{-2} is extracted out as P_{th} = 2.6 kW cm^{-2} at 78 K. Similarly, an electrically injected current density of ~0.28 kA cm^{-2} is extracted out as P_{th} = 0.13 kW cm^{-2} at 7.8 K.

Note S3. *E–k* dispersion of EPs and group index of light in a semiconductor microcavity

Based on Drude-Lorentz model, the dielectric function for an oscillator in a crystal could be expressed as:[3]

$$\varepsilon(E) = \varepsilon_b \left(1 + \frac{Ne^2}{\varepsilon_b m_0} \frac{\hbar^2 f}{E_T^2 - E^2 - iE\hbar\gamma}\right) \quad (3)$$

with ε_b the background dielectric constant, γ the damping constant, m_0 the free electron mass, $f = (E_L^2 - E_T^2) \cdot \frac{\varepsilon_b m_0}{\hbar^2 Ne^2}$ the oscillator strength, N the number of oscillator per unit volume, E_T and E_L the transverse and longitudinal resonance energies, respectively.

Additionally, for light propagating in a matter, the *E-k* dispersion could be obtained by equation:

$$E = \frac{c\hbar k}{n(E)} \quad (4)$$

Substituting eq (4) into eq (3) by $\varepsilon(E) = n^2(E)$, we can obtain:

$$E = \frac{\hbar c k_\parallel}{\sqrt{\varepsilon_b \left(1 + \frac{E_L^2 - E_T^2}{E_T^2 - E^2 - iE\hbar\gamma}\right)}} \quad (5)$$

E is the center energy of oscillation peaks in distal PL spectra in Figure 2 in the main text. $k_\parallel$ is the wavevector along *z* axis of NB, which can be expressed as $k_0 + n\pi/L$ (n = 1, 2, 3…), with k_0 an adjustable parameter. E_T equals exciton resonance energy E_0, which are 2.356 eV, 2.357 eV, 2.357 eV, and 2.352 eV at the temperatures of 295, 230, 140, and 78 K for the NB in Figure 2 in the main text, respectively. γ is extracted from in-situ PL and is equal to 67 meV, 50 meV, 31 meV, and 23 meV for CsPbBr$_3$ NB in Figure 2 in the main text at T = 295, 230, 140, and 78 K, respectively. The best fitting of ε_b is 4.6.[4] E_L can be fitted out and the coupling strength, Ω, can be further evaluated by determining the minimal vertical distance between LPB and UPB in the *E-k*$_\parallel$ dispersion.

For light propagating in a microcavity, the group index $n_g(E)$ could be extracted from the relation between $\Delta\lambda$ and λ, i.e., $\Delta\lambda = \lambda^2/(2Ln_g(E))$, where *L* is the cavity length. It can also be obtained from the *E-k* dispersions of EP using the formula demonstrated in Figure 2 in the main text.

Note S4. Rate equations for a laser in a semiconductor microcavity

In the rate equations, by assuming that one electron–hole pair is exchanged for one photon, the stimulated emission recombination is clearly shown as follows:[5]

$$\frac{\partial n}{\partial t} = R_{\text{ex}} - \frac{n}{\tau_{\text{SE}}} - S v_g g_m \quad (6)$$

$$\frac{\partial S}{\partial t} = -\frac{S}{\tau_p} + \Gamma v_g g_m S + \Gamma \beta \frac{n}{\tau_{\text{SE}}} \quad (7)$$

$$v_g g_m = \frac{an}{\tau_{\text{cav}}} \quad (8)$$

$$\beta = \frac{\tau_{\text{SE}}}{\tau_{\text{cav}}} \quad (9)$$

$$\tau_p^{-1} = \frac{\omega}{Q} \quad (10)$$

Where n is the total carrier density, S the photon density, R_{ex} is the optical pumping rate, τ_{SE}^{-1} is the spontaneous emission rate, Γ is the confinement factor, τ_p is the photon lifetime of the lasing mode, g_m is the material gain, v_g is group velocity, β is the spontaneous coupling factor, a is a coefficient, τ_{cav}^{-1} is the emission rate into the cavity mode, ω is the lasing frequency and Q is the quality factor of the mode.

Further, when laser occurs ($\frac{\partial S}{\partial t} = 0$) and neglecting the spontaneous emission term $\Gamma \beta \frac{n}{\tau_{\text{SE}}}$ in eq (7), we obtain the approximate threshold condition of a laser:

$$\Gamma v_g g_m - \frac{1}{\tau_p} = 0 \quad (11)$$

On the other hand, this threshold condition has to be consistent with the round-trip oscillation condition of an FP laser:

$$g_{\text{modal}} = \Gamma g_m^{\text{th}} = \frac{n_g}{n_r} \gamma' g_m^{\text{th}} > \alpha_m = \alpha_i + \alpha_c + \alpha_T = \alpha_i + \alpha_c + (1/L) \times (\ln(1/R)) \quad (12)$$

where g_{modal} is the modal gain, α_i is the intrinsic optical loss, α_c is the cavity loss, α_T the transmission loss at end-facets, and R indicates reflectivities at the two ends of the cavity.

$\Gamma = \dfrac{n_g}{n_r} \gamma'$ is the confinement factor, with γ' the energy density confinement in the material calculated from MODE (Lumerical, inc).

Combined with these equations, we obtain:

$$g_m^{th} = \frac{2\pi n_r}{Q \lambda_p \gamma'} = n_r \frac{\alpha_i + \alpha_c + (1/L) \times (\ln(1/R))}{\gamma' n_g} \quad (13)$$

where λ_p is the lasing wavelength.

Note S5. Calculations of material gain, modal loss, and threshold gain

Material gain. Based on Bernard-Duraffourg condition, to obtain positive material gain in semiconductor, it requires that the separation of quasi-Fermi levels of conduction and valence band exceeds photon energy, i.e., $F_C - F_V \geq E_g \geq h\nu$. And the material gain spectrum can further be expressed as:[5]

$$g(\hbar\omega) = \frac{\pi e^2}{n_r c \varepsilon_0 m_0^2 \omega} |M|^2 \int_0^\infty \rho_r (f_c - f_v) \frac{\hbar/\pi\tau_{in}}{(E_g + E - \hbar\omega)^2 + (\hbar/\tau_{in})^2} dE \qquad (14)$$

where c and ε_0 are the speed of light in vacuum and vacuum permittivity, respectively. M indicates the strength of the transition, which calculates from the momentum matrix element. f_c and f_v are Fermi distribution functions for electrons and holes, respectively. Besides, τ_{in} could be obtained via fitting the temperature dependent PL spectra and the results are shown in Figure S5c. ρ_r is reduced density of electronic states in a material, which can be simplified as:

$$\rho_r = \frac{1}{2\pi^2} (\frac{2m_r}{\hbar^2})^{3/2} \sqrt{\hbar\omega - E_g} \qquad (15)$$

where m_r is reduced effective mass. The required material parameters are listed as follow:

Materials parameters	CsPbBr$_3$
m_c	$0.15\,m_0$
m_h	$0.14\,m_0$
m_r	$0.072\,m_0$
$E_p(|M|^2 = \frac{m_0 E_p}{6})$	15.04 eV

Modal loss. Modal loss includes intrinsic optical loss α_i, cavity loss α_c, and transmission loss at end-facets α_T. α_c are obtained from MODE (Lumerical, inc), as shown in Figure S12. For α_i, it is exponentially decreased as temperature drops due to reduced carrier scattering effect, which could be expressed as $\alpha_i = \alpha_0 \exp(bT/E_u)$, where α_0 and b are constants, and E_u is the Urbach energy. α_T could be calculated as $\alpha_T = -\ln(\frac{n_p - 1}{n_p + 1})^2 / L$, with n_p the phase refractive index.

Note S6. Spontaneous emission factor β in a semiconductor microcavity

When stimulated emission occurs at laser threshold, we obtain $\dfrac{\partial n}{\partial t} = \dfrac{\partial S}{\partial t} = 0$, i.e.:

$$R_{ex} - \frac{n}{\tau_{SE}} - \frac{anS}{\tau_{cav}} = 0 \qquad (16)$$

$$-\frac{S}{\tau_p} + \Gamma \frac{anS}{\tau_{cav}} + \Gamma\beta \frac{n}{\tau_{SE}} = 0 \qquad (17)$$

Eliminating n, we can get:

$$R_{ex} = \frac{S}{\Gamma\tau_p(1+aS)}\left(\frac{1}{\beta} + aS\right) \qquad (18)$$

Eventually, β could be obtained via fitting the log-log curves in Figures 1 and 4 in the main text by eq (18).

Note S7. Is it a polariton laser for as-demonstrated CW laser in 1D CsPbBr$_3$ NB?

Here, we discuss whether the as-demonstrated CW laser in 1D CsPbBr$_3$ NB is polariton lasing. There are three evidences suggesting that the achieved CW laser might be a polariton laser.[6] First, as Figure 2 shown, the energy–out-of-plane (z-direction, long axis of NB) wavevector dispersions of the emitted photons from the end-facets above and below threshold both satisfy the polariton model.[6] Second, the excitation density at laser threshold is below the Mott density. Third, a blue shift of the laser modes was observed as increase the power density (Figure S15), which may be due to a reduced exciton binding energy and weakened oscillator strength by carrier screening.[7, 8] However, the energy–in-plane wavevector (x, y direction, perpendicular to the long axis of NB) dispersion relation for a polariton laser should also satisfy the polariton model; this criterion is widely used for demonstrating the polariton condensation and lasing for the vertical semiconductor microcavity confined by two DBRs.[7, 8] However, for the one dimensional NBs or NWs, it is a challenge to detect the in-plane wavevector of photons because that the wavevectors of emitted photons are modified owing to the diffraction effect. Therefore, whether as-demonstrated CW laser is polariton laser is not clear and we utilize an EP modified laser model to describe the laser mechanism in the main text.
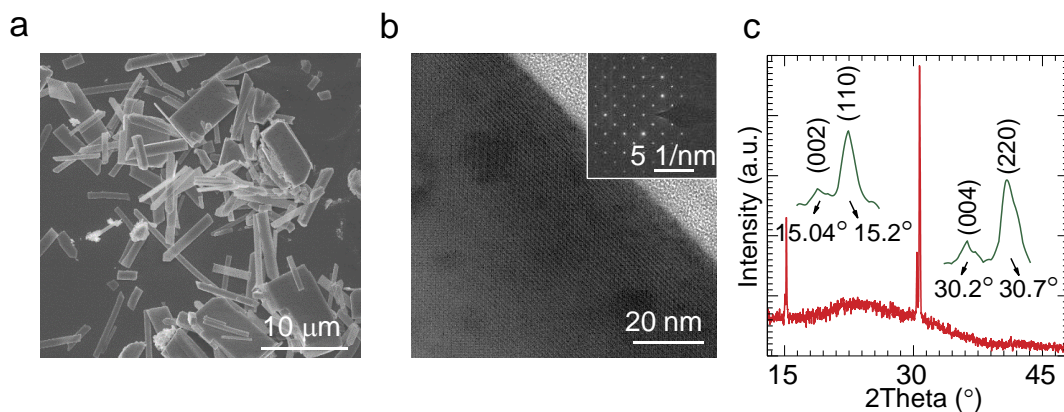
Figure S1. (a) Scanning electron microscope (SEM) image of as-grown solution-processed CsPbBr$_3$ NBs. (b) High resolution transmission electron microscopy (HRTEM) image and selected area electron diffraction patterns (SEAD) of as-grown CsPbBr$_3$ NB show the single crystal nature. (c) X-ray diffraction (XRD) spectrum of as-grown CsPbBr$_3$ NBs. Four peaks are resolved at ~ 15.04°, 15.2°, 30.2°, and 30.7°, which are indexed to (002), (110), (004), and (220) of orthorhombic phase CsPbBr$_3$ (ICSD 97851), respectively.
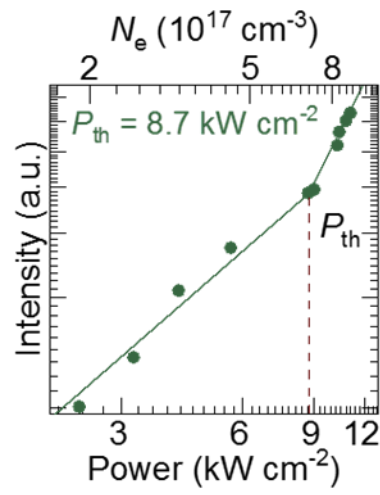
Figure S2. The *log-log* scale integrated intensity versus power density (excitation density) for a NB at 78 K with a P_{th} of 8.7 kW cm^{-2}.
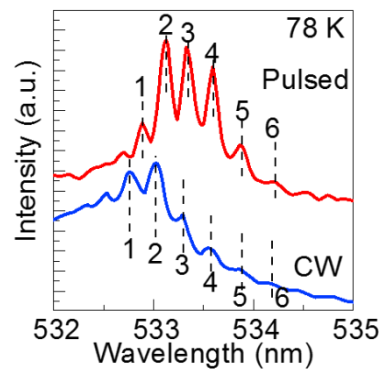
Figure S3. The lasing spectra of a CsPbBr$_3$ NB under CW and pulsed laser excitation at 78 K. The spectra are quite similar.
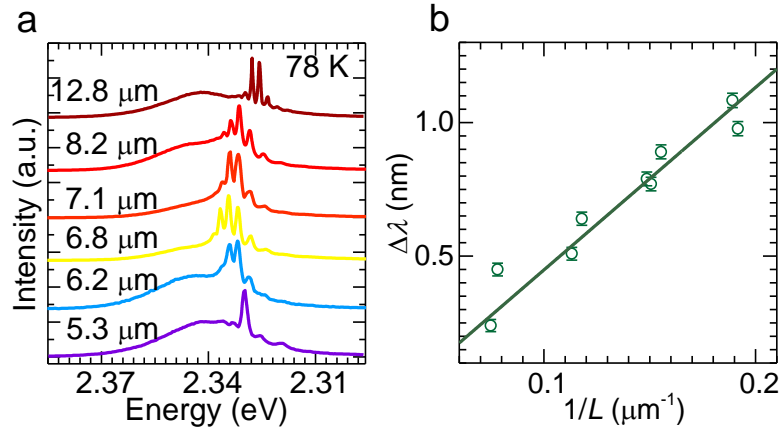
Figure S4. (a) Size-dependent CW laser emission of as-grown CsPbBr$_3$ NBs at 78 K. (b) Free spectral range $\Delta\lambda$ is inversely linear to L, which confirms longitudinal Fabry–Pérot (F–P) oscillation along long axis of CsPbBr$_3$ NBs.
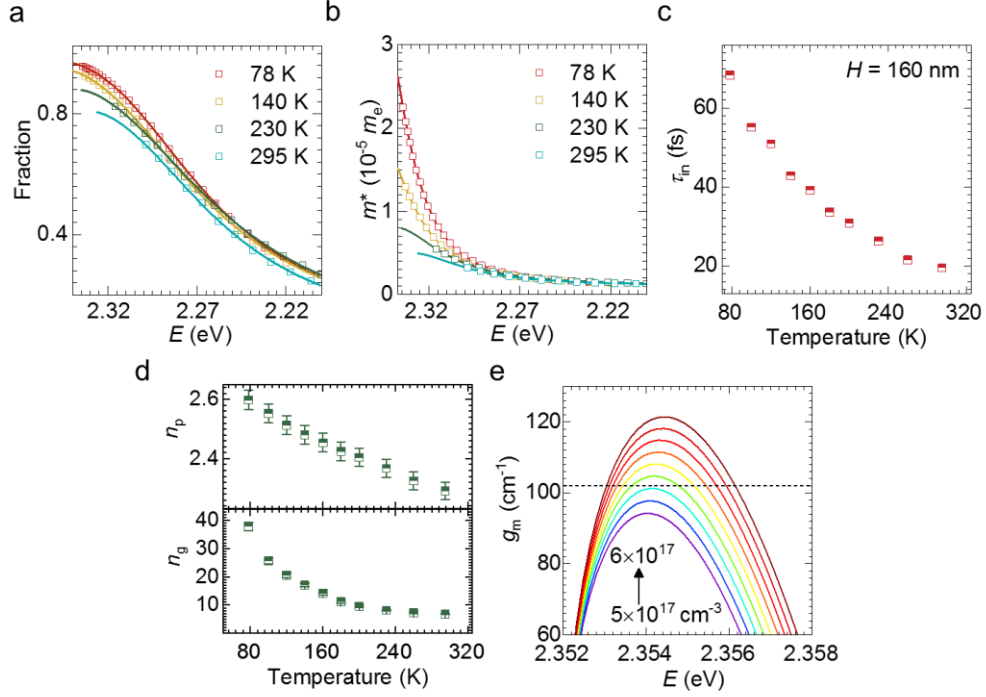
Figure S5. Temperature dependent exciton fraction (a) and effective mass (b) of EPs in LBP for the CsPbBr$_3$ NB in Figure 2 in the main text. (c) The calculated temperature dependent intraband carrier scattering lifetime for the CsPbBr$_3$ NB in Figure 2. (d) Temperature-dependent n_p and n_g for NB in Figure 2 in the main text. (e) Excitation density-dependent material gain spectra under 78 K for the CsPbBr$_3$ NB in Figure 2 in the main text. The optical pumped excitation density ranges from 5×10^{17} to 6×10^{17} cm^{-3}. The black dashed line indicates the required material gain (102 cm^{-1}).
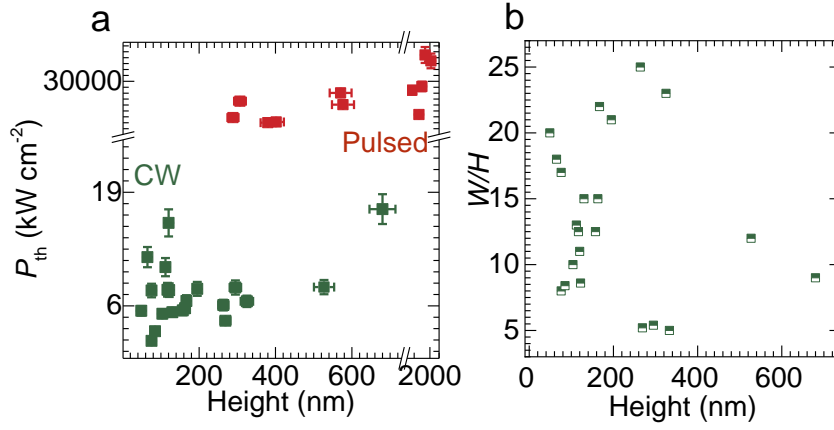
Figure S6. (a) Height-dependent lasing thresholds of CsPbBr$_3$ NBs, showing that the CW lasing mainly occurs when the height is < 400 nm. The lateral error bars indicate the variations for the heights of NBs obtained from AFM measurement. The longitudinal error bars suggest the variations for laser thresholds obtained from the power meter. (b) Height-dependent width/height ratio of CsPbBr$_3$ NBs, showing that the CW lasing occurs when the ratio is about ~10-15.
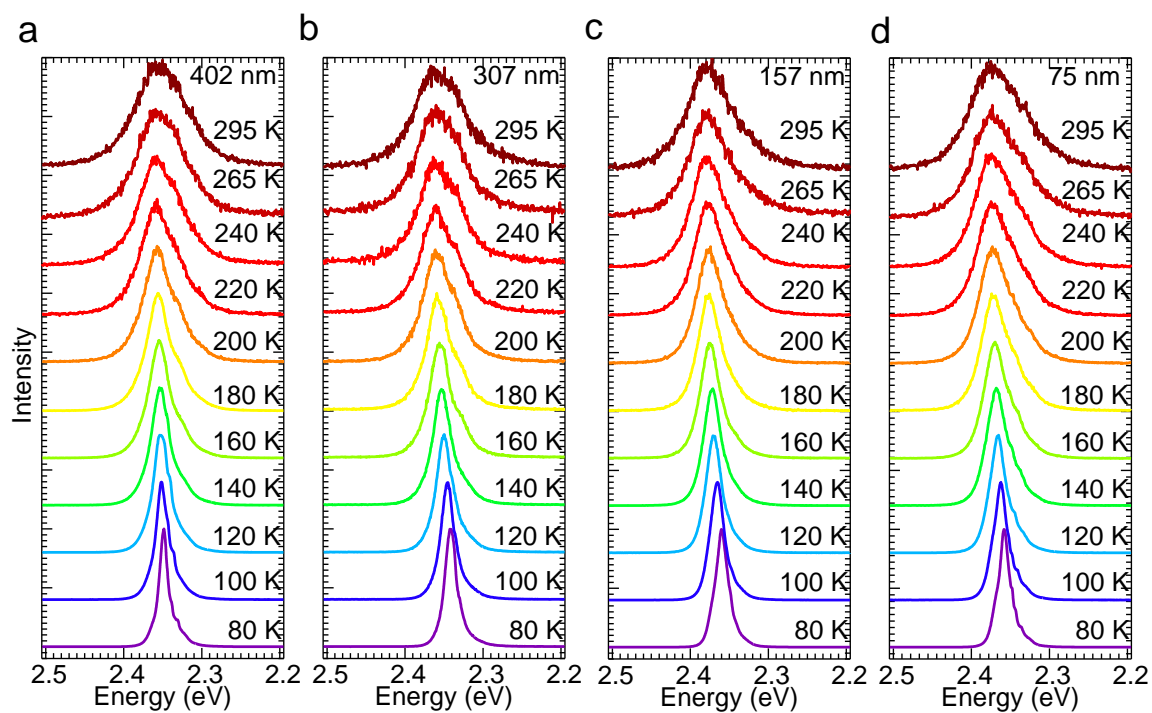
Figure S7. Temperature-dependent PL spectra for four representative CsPbBr$_3$ NBs in Figure 3 in the main text under the excitation of 405 nm CW laser.
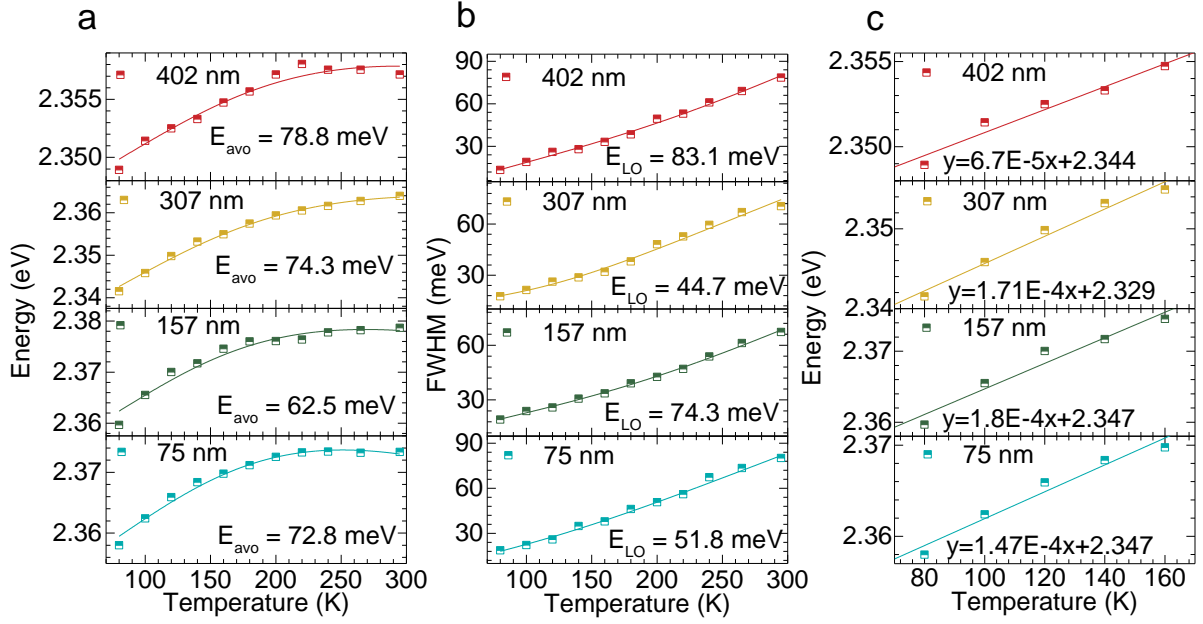
Figure S8. (a) Average optical phonon energy estimated by the equation:

$$E_{g}(T)= E_{0} + A_{TE}T + A_{EP}\left(\frac{2}{\exp(E_{avo}/k_{B}T-1)}+1\right),$$ where E_{0} is the bandgap at 0 K, A_{TE} and A_{EP}

represent the proportion of contribution from the thermal expansion (TE) and electron-phonon coupling, respectively, E_{avo} represents the average optical phonon energy. (b) Longitudinal

optical phonon energy estimated by the equation: $\Gamma(T)= \Gamma_{0} + A_{a-ph}T + \Upsilon_{LO}(\exp(E_{LO}/k_{B}T-1))^{-1}$,

where Γ_{0} represents the T-independent inhomogeneous broadening term, A_{a-ph} is the

exciton-acoustic phonon coupling coefficient, Υ_{LO} and E_{LO} represent the electron-phonon

interaction strength and the LO phonon energy. (c) Estimated A_{TE} for four representative

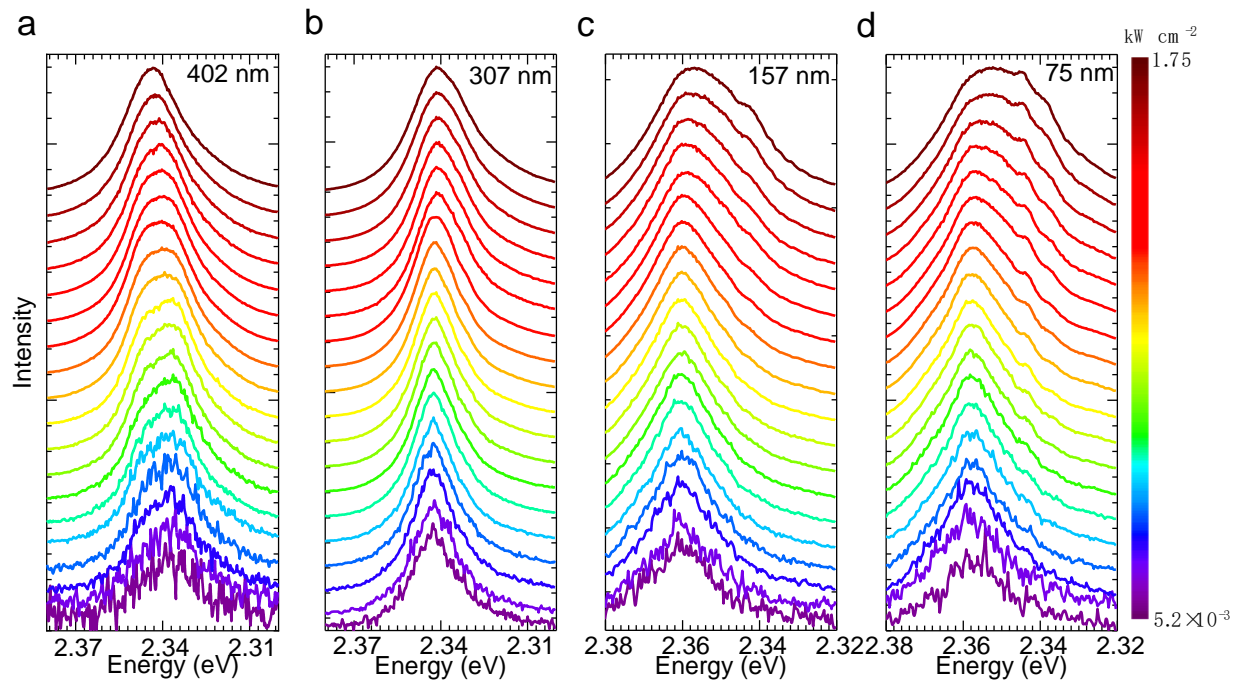CsPbBr$_3$ NBs in Figure 3 in the main text.

Figure S9. Power density-dependent PL spectra for four representative CsPbBr$_3$ NBs in Figure 3 in the main text under 405 nm CW laser excitation at 78 K. Power density is ranging from 5.2 × 10^{-3} to 1.75 kW cm^{-2}.
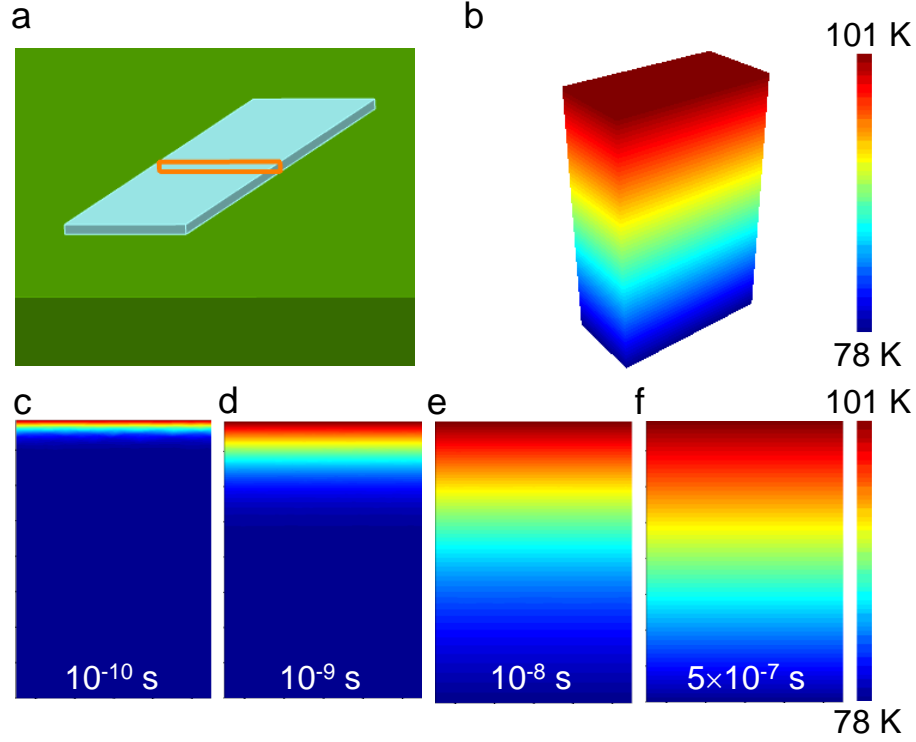
Figure S10. (a) Schamtics of thermal diffusion simulated by DEVICE (Lumerical, inc). Heat source is settled at zero time ($t = 0$ s, time revolution: 10^{-10} s). The differentials between 78 K and heat source is twice the differentials between 78 K and the average temperature of NBs measured in Figure 3d in the main text. (b) The simulated equilibrium temperature distribution for a representative CsPbBr$_3$ NB with length $\times$ width $\times$ height = $10.0 \times 2.0 \times 0.157$ μm. (c)-(f) Time-dependent 2D pseudo-color plots (*x-y* plane) temperature distribution for a representative CsPbBr$_3$ NB with length $\times$ width $\times$ height = $10.0 \times 2.0 \times 0.157$ μm.
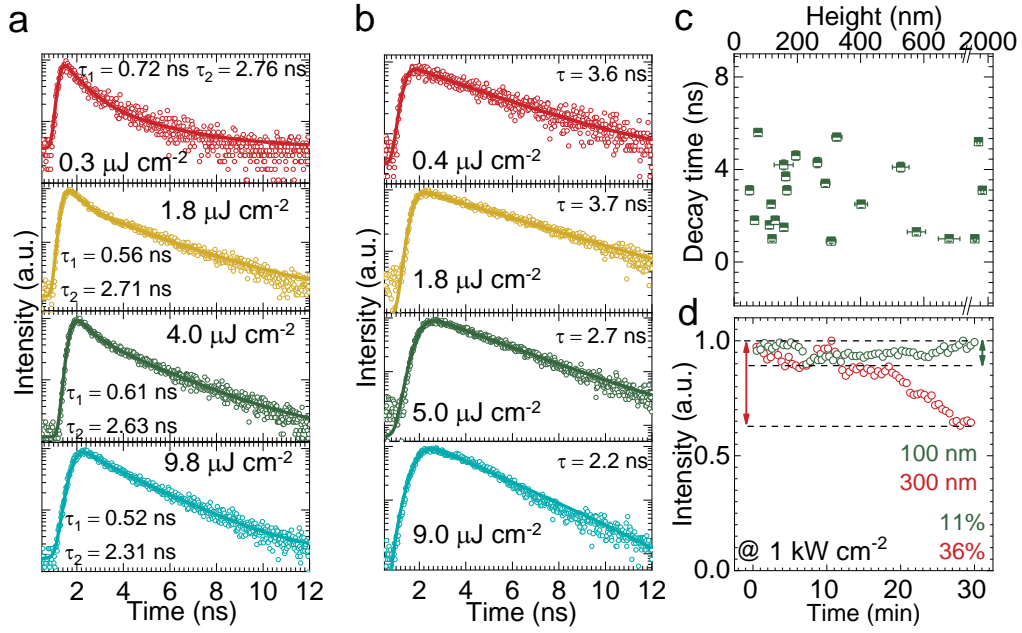
Figure S11. Room temperature pump pulse fluence-dependent TRPL spectra of representative CsPbBr$_3$ NBs with the height of 402 nm (a) and 75 nm (b), respectively. (c) Height-dependent lifetimes of CsPbBr$_3$ NBs. (d) The photonstability for CsPbBr$_3$ NBs with heights of ~100 and 300 nm, respectively, on the sapphire substrate under CW excitation with a power density of 1.0 kW cm^{-2} at 78 K.
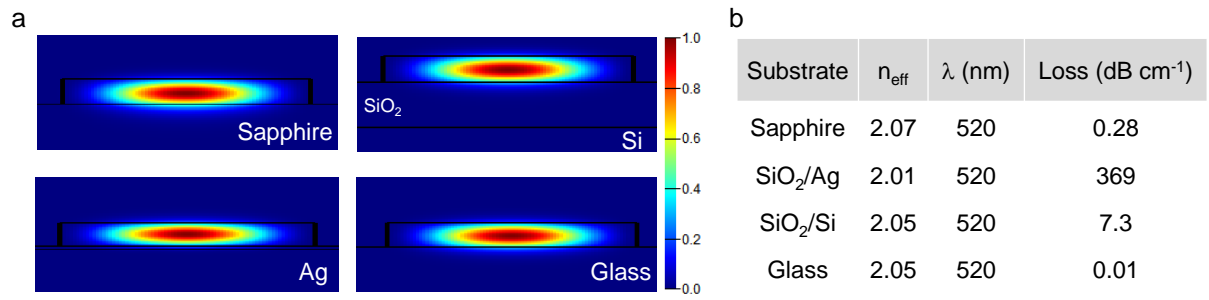
a

b

Substrate	n_{eff}	λ (nm)	Loss (dB cm^{-1})
Sapphire	2.07	520	0.28
SiO$_2$/Ag	2.01	520	369
SiO$_2$/Si	2.05	520	7.3
Glass	2.05	520	0.01

Figure S12. (a) Simulated mode distribution for NBs with length × width × height = 10.0 × 2.0 × 0.40 μm on selected substrates by MODE (Lumerical, inc). No photonic mode exists at ~517 nm on Si substrate without SiO$_2$ spacer. (b) Corresponding photonic parameters of fundamental mode in (a). The high dielectric function of Ag and Si substrates causes a higher cavity loss.
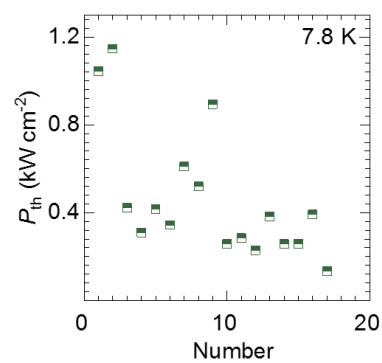
Figure S13. The thresholds of 17 CsPbBr$_3$ NBs under CW excitation at 7.8 K. The threshold ranges from 0.13 to 1.14 kW cm^{-2}.
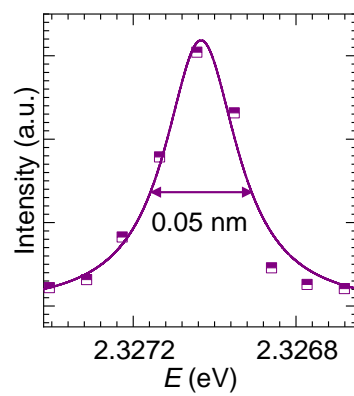
Figure S14. Lorentz function fitted lasing emission shows a linewidth of 0.05 nm at 532.9 nm for P = 7.9 mW or 1.4 kW cm^{-2} under 7.8 K.
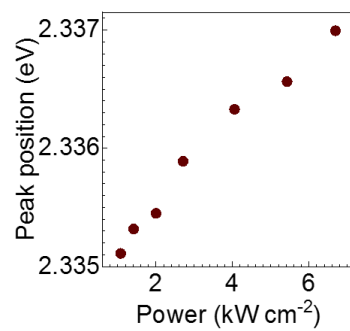
Figure S15. Power density dependent peak energy of a laser mode at 2.335 eV for the NB in Figure 1c.

Table S1. A comparison of our work with CW pumped laser based on perovskite materials in previous literatures.

Materials	Method	Cavity	Temperature	Lasing/ASE	P_{th}	FWHM (nm)	Ref.
MAPbI$_3$ film	spin-coating	DFB	102 K	lasing	17 kW cm^{-2}	0.25	[9]
MAPbI$_3$ film	spin-coating	W/O	80 K	ASE	387 W cm^{-2}	2	[1]
MAPbI$_3$ film	spin-coating	DFB	RT	lasing	13 W cm^{-2}	0.7	[10, 11]
CsPbBr$_3$ NW	solution-phase synthesis	F-P	78 K	lasing	6 kW cm^{-2}	0.23	[6]
CsPbBr$_3$ NW	anti-solvent method	F-P	78 K	lasing	2.6 kW cm^{-2}	0.3	this work
CsPbBr$_3$ NW	anti-solvent method	F-P	7.8 K	lasing	134 W cm^{-2}	0.05	this work

REFERENCES

1. Brenner, P.; Bar-On, O.; Jakoby, M.; Allegro, I.; Richards, B. S.; Paetzold, U. W.; Howard, I. A.; Scheuer, J.; Lemmer, U. Continuous wave amplified spontaneous emission in phase-stable lead halide perovskites. *Nat. Commun.* **2019**, *10*, 1-7.

2. Leyden, M. R.; Terakawa, S.; Matsushima, T.; Ruan, S.; Goushi, K.; Auffray, M.; Sandanayaka, A. S.; Qin, C.; Bencheikh, F.; Adachi, C. Distributed feedback lasers and light-emitting diodes using 1-naphthylmethylamnonium low-dimensional perovskite. *ACS Photonics* **2019**, *6*, 460-466.

3. van Vugt, L. K.; Piccione, B.; Cho, C. H.; Nukala, P.; Agarwal, R. One-dimensional polaritons with size-tunable and enhanced coupling strengths in semiconductor nanowires. *Proc. Natl. Acad. Sci. U. S. A.* **2011**, *108*, 10050-10055.

4. Shang, Q.; Li, C.; Zhang, S.; Liang, Y.; Liu, Z.; Liu, X.; Zhang, Q. Enhanced optical absorption and slowed light of reduced-dimensional $CsPbBr_3$ nanowire crystal by exciton–polariton. *Nano Lett.* **2020**, *20*, 1023-1032.

5. Chen, R.; Tran, T.-T. D.; Ng, K. W.; Ko, W. S.; Chuang, L. C.; Sedgwick, F. G.; Chang-Hasnain, C. Nanolasers grown on silicon. *Nat. Photonics* **2011**, *5*, 170-175.

6. Evans, T. J. S.; Schlaus, A.; Fu, Y.; Zhong, X.; Atallah, T. L.; Spencer, M. S.; Brus, L. E.; Jin, S.; Zhu, X. Y. Continuous-wave lasing in cesium lead bromide perovskite nanowires. *Adv. Opt. Mater.* **2017**, *6*, 1700982.

7. Kasprzak, J.; Richard, M.; Kundermann, S.; Baas, A.; Jeambrun, P.; Keeling, J. M. J.; Marchetti, F. M.; Szymańska, M. H.; André, R.; Staehli, J. L.; Savona, V.; Littlewood, P. B.; Deveaud, B.; Dang, L. S. Bose–Einstein condensation of exciton polaritons. *Nature* **2006**, *443*, 409-414.

8. Das, A.; Heo, J.; Jankowski, M.; Guo, W.; Zhang, L.; Deng, H.; Bhattacharya, P. Room temperature ultralow threshold GaN nanowire polariton laser. *Phys. Rev. Lett.* **2011**, *107*, 066405.

9. Jia, Y.; Kerner, R. A.; Grede, A. J.; Rand, B. P.; Giebink, N. C. Continuous-wave lasing in an organic–inorganic lead halide perovskite semiconductor. *Nat. Photonics* **2017**, *11*, 784-788.

10. Li, Z.; Moon, J.; Gharajeh, A.; Haroldson, R.; Hawkins, R.; Hu, W.; Zakhidov, A.; Gu, Q. Room-temperature continuous-wave operation of organometal halide perovskite lasers. *ACS Nano* **2018**, *12*, 10968-10976.

11. Brenner, P.; Paetzold, U. W.; Turnbull, G. A.; Giebink, N. C.; Samuel, I. D. W.; Lemmer, U.; Howard, I. A. Comment on "Room-temperature continuous-wave operation of organometal halide perovskite lasers". *ACS Nano* **2019**, *13*, 12257-12258.